

Department of Meteorology, University of Belgrade, Serbia

The 3-D model characteristics of a Cb cloud which moves along a valley

M. Ćurić, D. Janc, D. Vujović, and V. Vučković

Received June 2002; revised August 22, 2002; accepted October 1, 2002
Published online: April 10, 2003 © Springer-Verlag 2003

Summary

The three-dimensional cloud-resolving mesoscale model is used to simulate an individual Cb cloud in condition of real orography. We have conducted our numerical experiments over an area known as hail bearing clouds source. Once formed such clouds regenerate and propagate along the valley if the shallow layer of strong wind shear exists. The orographic effects on model Cb cloud are recognized through comparison of simulated cloud characteristics with those calculated for the flat terrain. Sensitivity experiments with respect to the wind shear layer depth are also conducted.

Our results demonstrate the model capability to simulate well some observational Cb cloud characteristics. It is shown that the river valley is of essential importance for Cb cloud development. The most prominent features of the model cloud in this case are as follows: fast propagation along the river valley; considerable depth of the cold air nose with pronounced pulsation mechanism and intense cell regeneration at the leading edge of cold air outflow. Model and observed radar reflectivities in the vertical cross-section are in agreement. Some characteristics of surface cumulative rain precipitation are also well reproduced by the model. In contrast with the real orography case, the model cloud is more intense and it propagates freely in lateral direction for the flat terrain. The cell regeneration associated with forced updraft above the cold air nose is not pronounced in contrast with earlier considerations. Reflectivity pattern near the ground, having mainly “bat-like” wings, encircles much larger area with altitude compared to the case of real orography. Finally, the model cloud characteristics depend strongly on shear layer.

1. Introduction

The Cb cloud characteristics for real orography is treated only sporadic in literature. According to observational evidence (Ćurić, 1980; 1982; 1987) the immediate environment west of the Western Morava valley (especially Zlatibor plateau) is known as hail bearing clouds source. Namely, hail suppression projects conducted over three decades in Serbia show that such clouds along the Western Morava valley cause extensive damage to property. The aim of this work is to explore some aspects of this behavior.

Ćurić (1982) established the conceptual model of such clouds based on numerous radar data and observations at the ground. According to this model, a cloud is formed on the mountain plateau. At the next phase, it moves down from a plateau into the valley under the strong directional wind shear at low-levels even though the atmosphere is not very unstable and need not have too large amount of moisture. Such cloud behavior is observed when the environmental mid-tropospheric wind is nearly parallel to the valley and the low-level air motion is from the opposite direction. A strong downdraft occurs since the land slopes down to a valley. The local

low pressure and the forced lifting of a warm air above the cold air amplify the warm air motion towards the mountain side. The strong updraft associated with the cold air nose in front of a cloud occurs. The cold air nose formed pulsates in time and the leading edge of the nose is close to the mother cloud due to relationship between pressure gradient force and surface friction, which in turn, lead to direct inflow of lifted warm air into the main updraft of the mother cloud. At the leading edge of the cold air nose, the daughter cloud forms and it is merged by the mother cloud. Observed Cb cloud propagates and regenerates rapidly due to the channeling effect. So, Čurić (1982) observed that the apparent cloud propagation speed was 55 km/h.

In recent years the cloud resolving mesoscale models became capable of simulating many observed characteristics of an individual Cb cloud. In this period, some numerical studies (Fovell and Tan, 1996; Lin et al, 1998) treated storm propagation and cell regeneration mechanism of the mother cloud. Lin et al (1998) concluded that the principal mechanism of cell regeneration within multicell storm was the advection in agreement with Čurić (1982), who had used an other terminology. Lin et al (1998), and Lin and Joyce (2001) simulations were performed over a plateau where the cloud propagation velocity was a factor of more than 3 smaller than that observed in the Western Morava valley. Fovell and Tan (1996) pointed out the pulsating mechanism of a storm.

The primary aim of our paper is to give more complete insight into characteristics of an individual Cb cloud moving along a river valley in mountainous region as well as to detect the most pronounced differences compared to those obtained for the flat terrain.

2. Description of the model

The three-dimensional mesoscale model used for cloud simulation is the Advanced Regional Prediction System (ARPS) version 4.0. This model has been developed by CAPS (Center for Analysis and Prediction of Storms) at the University of Oklahoma. Many papers (e.g., Johnson et al, 1994; Droegemeier et al, 1995; Xue, Droegemeier and Wong, 2000; Xue et al, 2001) describe the model in more details. The ARPS-model numerically integrates the

time-dependent, non-hydrostatic and fully compressible equations.

The model uses the generalized terrain-following coordinate in the vertical, while the horizontal coordinates are the same as in the Cartesian system. Such irregular grid transformed to rectangular computational grid using two steps: terrain-following coordinate transformation and vertical grid stretching.

The prognostic variables of the model are: Cartesian wind components, perturbation potential temperature and pressure, turbulent kinetic energy and mixing ratios for water vapour, cloud water and ice, rainwater, snow and hail.

The spatial discretization is made on Arakawa C-grid. The horizontal and vertical advection of momentum and scalars is treated by fourth-order quadratically-conservative finite differences. The other terms are treated by second-order differencing. The second-order leap-frog scheme is used for large time steps, while the first-order forward-backward explicit scheme is used for small time steps. Large time step size is associated with the integration of the non-acoustic wave modes. Acoustic waves are integrated inside the small time step by using a mode splitting technique. Hereafter, the respective time steps of 6s and 2s are used. The wave-radiating condition is applied for lateral boundaries in order to allow waves to pass out freely through the boundary with minimum of reflection. The radiation condition for the top of the domain and the rigid one for the bottom boundary are used. Top radiation condition uses a Rayleigh spongy layer near the top boundary in order to absorb upward propagating wave disturbances and prevent wave reflection at the top boundary. Rayleigh damping coefficient (s^{-1}) in the spongy layer is $v(z) = 0.5v_t\{1 - \cos[\pi(z - z_1)/(z_t - z_1)]\}$, where v_t is the maximum Rayleigh friction coefficient taken to be $0.0083 s^{-1}$ (inverse of v_t is 20 times large time step), while z_t and z_1 are heights of the top boundary and the bottom of the spongy layer, respectively. In calculations we set $z_1 = 10.5$ km.

The turbulence is treated by 1.5-order turbulent kinetic energy formulation. In our calculations the constant drag coefficients for momentum stresses, turbulent heat flux and turbulent moisture flux at the ground are used. The radiation is also included. Coriolis force is neglected.

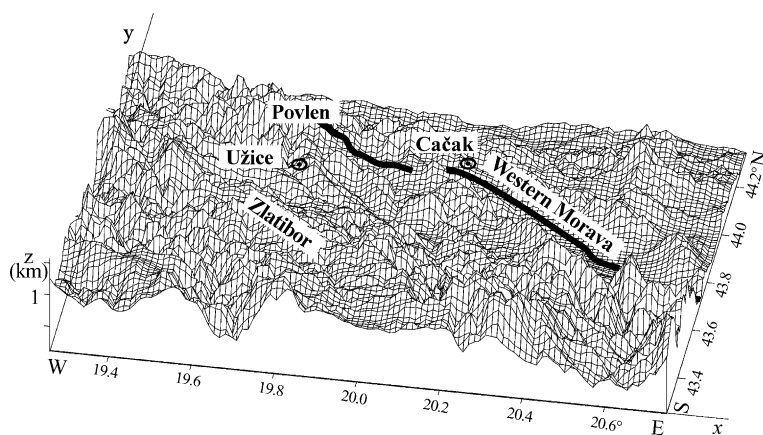


Fig. 1. The three-dimensional topography of the western Morava valley with its surroundings within model domain. The x-, y- and z-directions are shown

The model cloud microphysics includes the initiation of cloud water and cloud ice as well as interactions between cloud water, cloud ice, rain and snow in agreement with Lin et al (1983). Hail accretion formulas are employed in accordance with Ćurić and Janc (1996; 1997), while hail melting and sublimation terms are those as proposed by Ćurić et al (1999). The hail terms used treat only hail-sized particles (an equivalent sphere diameter equal and greater than 0.5 cm; realistic hail spectrum) instead of those with diameters between 0 and ∞ (idealized hail spectrum). Such hail production terms differ from Lin et al (1983) ones for the coefficients including incomplete gamma functions, which in turn, lead to significantly different values compared to former ones (factor of more than 3).

The ARPS-model has two terrain options: analytic mountain and terrain data sets. We therefore choose it for the treatment of an individual Cb cloud in condition of real orography. In this case we use the terrain data $30'' \times 30''$ ($0.65 \times 0.65 \text{ km}^2$) covering Serbia and Montenegro with their surroundings.

The reference state is homogeneous in the horizontal using a single sounding giving the values of temperature, humidity, pressure, wind velocity and direction. The model cloud is initiated by introducing a ellipsoidal warm bubble with 5 K amplitude in its center having a horizontal radius of 10 km and a vertical radius of 1.5 km.

Three-dimensional topography of the Western Morava valley with its mountainous environment is presented in Fig. 1 in degrees of geographical longitude and latitude. The center of considered area is at 43.8° N and 20° E , while its mean height above sea level is about 300 m. Between Požega

and Čačak, the valley width is only a few hundred meters (Ovčar-Kablars' cliff). Orientation of the valley is almost northwest-southeast. The valley is flanked by high mountains. Its floor is flat and very narrow, especially in the middle part.

Figure 1 shows the full model domain along x- and y-axis. Equivalent distances (in km) are 112 km in the x- and y-directions, while the height of the top boundary is 16 km. Space resolution of the model is 1000 m in the horizontal and 500 m in the vertical. Despite a fact that this resolution is rather coarse, we have in mind that two conditions are satisfied: available computer resources and the model capability to simulate well the processes considered in the paper. The simulations were terminated at 120 min.

The coordinates of the warm bubble center are $(x, y) = (32, 96)$ km in the horizontal and 1.5 km in the vertical above the Povlen mountain (peak height of 1350 m).

3. Analysis of model results

In this section, we demonstrate the model capability to simulate well an individual Cb cloud under condition of real orography. According to observational evidence (Ćurić, 1982; 1987), we simulate at first an individual Cb cloud moving along the Western Morava valley under shallow layer of strong shear referred to as Case A. In order to detect the orographic impact on Cb cloud development we compare results of two model runs (A1 and A2) relating to real orography and flat terrain, respectively. We expect that Run A1 describes the most frequent behavior of an individual Cb cloud in the considered area (Ćurić, 1982). However, observations detect

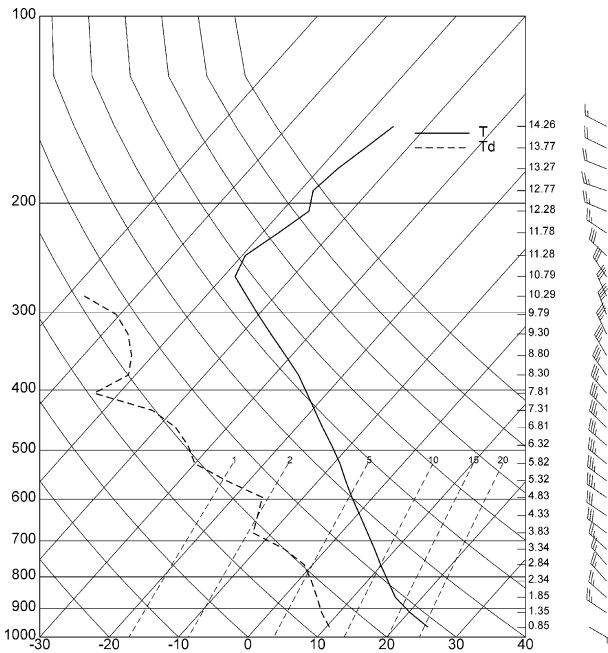


Fig. 2. Rawinsonde balloon sounding of 13th June 1982 at 10 00 of local time

some other individual Cb clouds which also initiate in the mountainous region west of the valley. The first ones associated by deep layer of wind shear donot propagate far from their source. An example of such cloud is simulated by Case B. The other ones are the short-lived clouds moving with mid-tropospheric wind independently on the valley axis. The atmosphere in which they initiate is characterized by weak-sheared hodograph. Case C simulates a such cloud.

For case A the initial input data were taken from the local sounding of 13th June 1982 at 10 00 with corresponding wind profile (Fig. 2). As noted, the wind direction veered sharply from south-east to north-west above 750 m. The wind speed increased with altitude from around 7 m/s near the surface to about 17 m/s at 9 km MSL. As noted, the atmosphere is nearly stable and without large moisture amount. The local conditions were favourable for an individual Cb cloud formation according to Čurić (1982). Cases B and C use the initial soundings with same temperature and dew point profiles, while the wind has the same magnitudes as in Case A. Only difference compared to A case is that the wind is from the south-east to nearly 2 km for B case, while the wind is always from the northwest for C one.

3.1 Case A

At first we investigate the model cloud characteristics when it moves along the river valley (Run A1). Among several ways of cloud fields presentation we select reflectivity and flow patterns depicted at $z = 1$ km (near ground) for different times (Fig. 3). Figure 3a–f refers to 15 min time intervals beginning at $\tau = 45$ min (simulated time). After being initialized at $\tau = 15$ min over Povlen mountain the model cloud grows and propagates in NW–SE direction towards the western Morava valley. Because of the steep slope of mountain sides, the cloud moves down rapidly into the valley. After $\tau = 45$ min (Fig. 3a) the cloud is in the valley. Within the next 15 min, the cloud propagation speed is about 45 km/h in NW–SE direction.

The cell initiated at the front part of the mother cloud is denoted by “1”. The updraft associated with it we call “main updraft”. At the mother cloud flank sides, two separate convective cells denoted by numbers “2” and “3” with opposite signs of vorticity can be observed. The vorticity mechanism within a storm is elaborated by many authors, e.g. Toutenhoofd and Klemp (1983), Davies-Jones (1982) or Droegemeier and Lazarus (1993). Hereafter we should not explain the mechanism of vortex formation but only the orographic impact on its development. Comparison of Fig. 3b and c indicates that the cloud motion accelerates with time. Both cells “2” and “3” intensify.

In order to better understand the mother cloud propagation and regeneration, we also depict vertical velocities and the cold air nose in vertical cross-section through the storm along straight line (as shown in Fig. 3) for selected time intervals in Fig. 4. Beneath the cloud base, the cold air nose (interface between cold air outflow and environmental warm air) is formed (Fig. 4a). Its leading edge propagates not far from the mother cloud due to surface friction. This causes continual regeneration of cell “1” induced by low-level convergence ahead of the cold air nose and its fast propagation along a valley axis as elaborated by Čurić (1982). Within next 15 min the height of the gust front nose increases (Fig. 4b). The peak updraft speed of 25.3 m/s is observed. Further, the leading edge of the cold air nose continues to lie close to the mother cloud. The cold air nose height regularly increases and decreases with

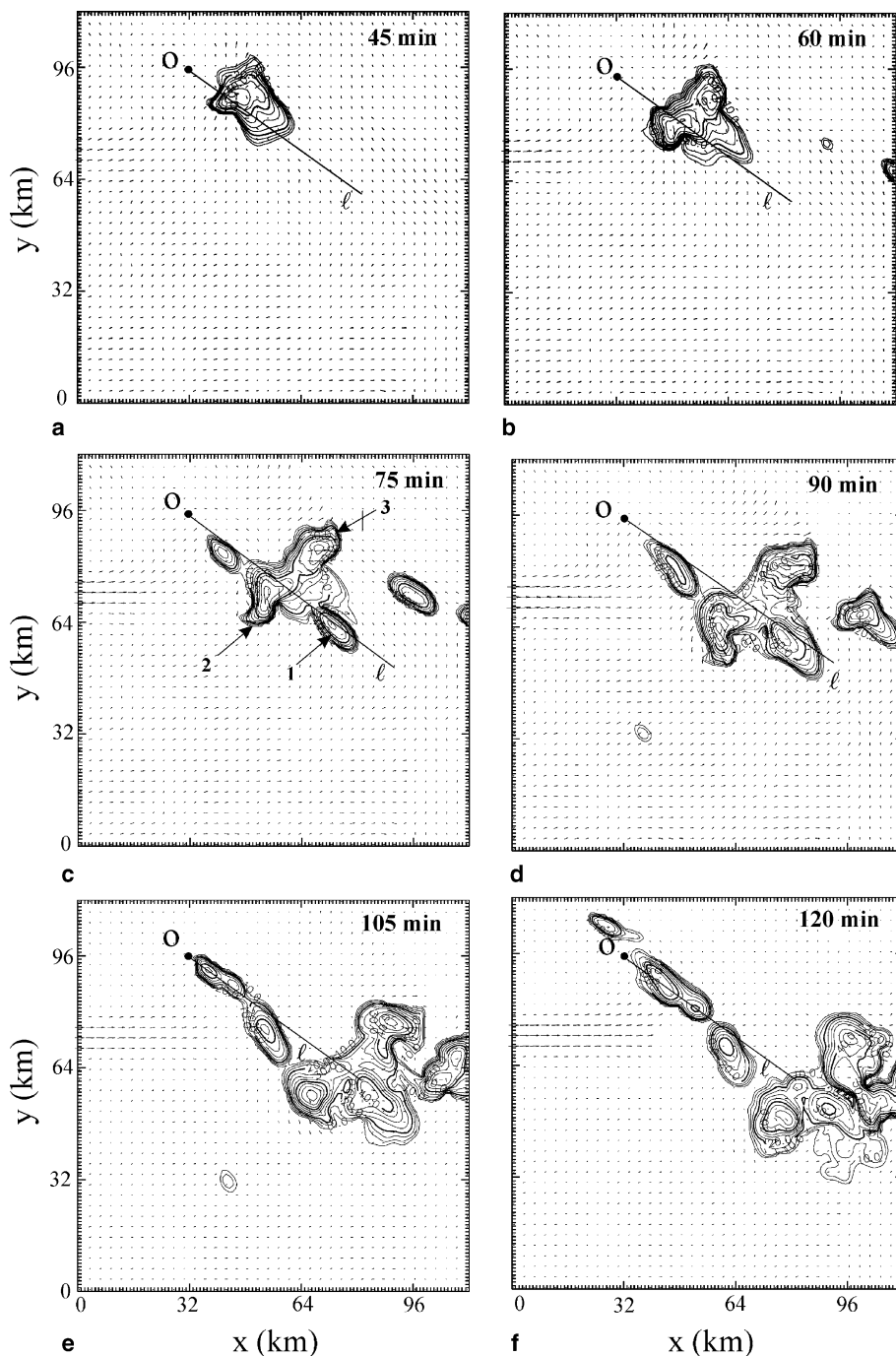


Fig. 3. Evolution of reflectivity (dBZ) and wind (m/s) depicted on horizontal plane at $z = 1$ km for Run A1. Figure 3a–f relates to 15 min time intervals beginning at $\tau = 45$ min. The axes x and y are in km. Solid line at each plot (l -axis; oriented along the Western Morava valley) indicates the location of vertical cross-section presented in Fig. 4. The point “O” denotes location of the initial bubble perturbation center. Numbers 1–3 in Fig. 3c denote cells at the front part of the mother cloud and those with opposite sign of vorticity, respectively

time (Fig. 4d–f). As a consequence, the vertical velocity also changes periodically (corresponding maxima of 25.3, 9.4, 14.5, 7.14 and 10.9 m/s, Fig. 4b–f). This leads to the strong forced inflow of the warm air through the cloud base. Since the cold nose propagates rapidly along the valley, the warm air can be lifted high up. The distance between the leading edge of the cold air nose and the main updraft is about

10 km. The wave-like cold air nose formed by precipitation evaporation also remains in the valley considerably behind the mother cloud.

Within 30 min up to $\tau = 120$ min (Fig. 3d–f), three new cells aligned along the valley axis are formed behind the mother cloud above the places where the slope of the boundary between cold and warm air changes sharply. The peak reflectivity values within the mother cloud

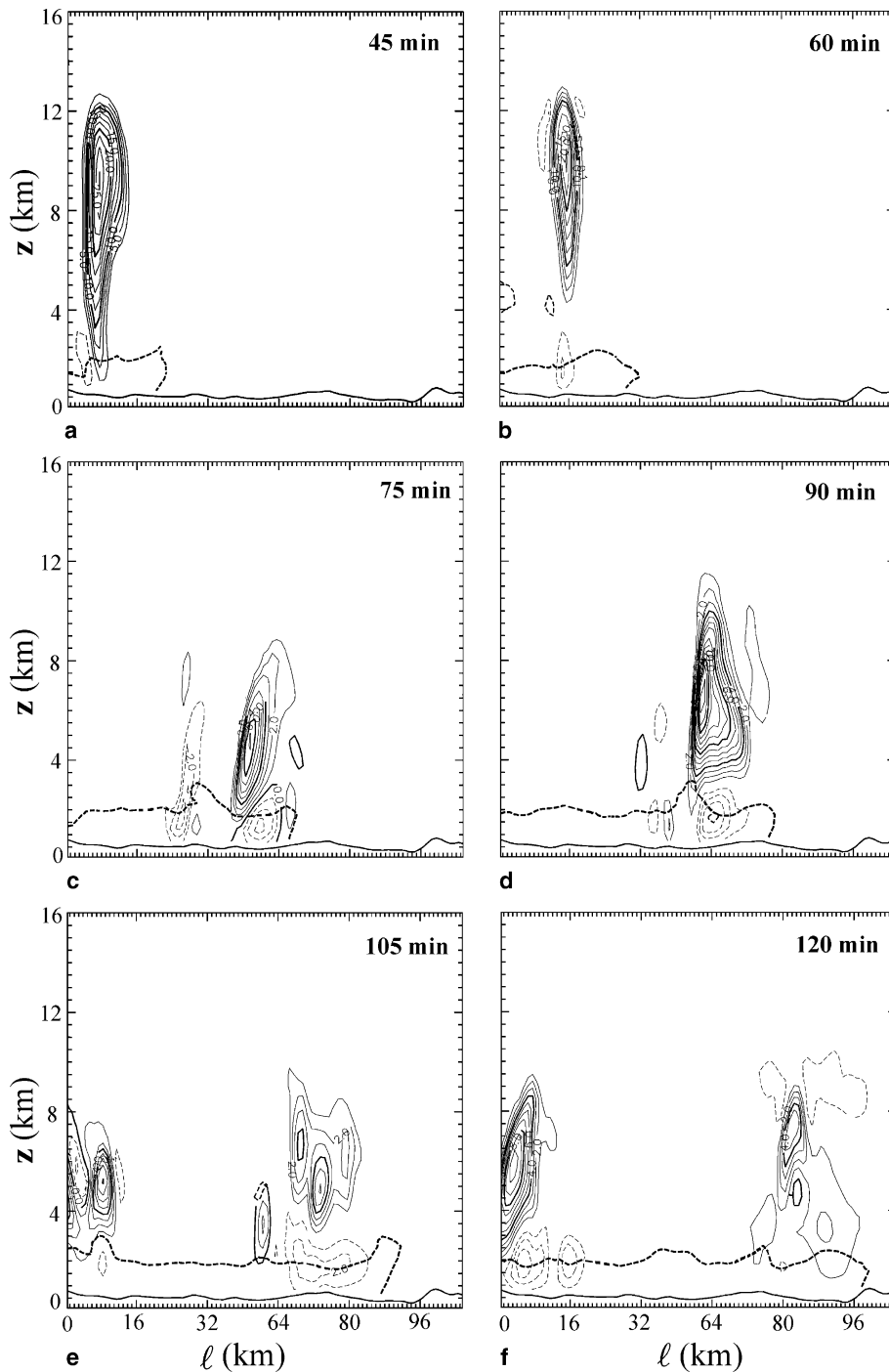


Fig. 4. Evolution of vertical velocities (m/s) for Run A1. Gust front nose is denoted by thick dashed line (potential temperature perturbation is -0.1 K). Figure 4a–f relates to the same time intervals as in Fig. 3. The l - and z -axes are in km

vary slightly (from 55.4 to 57.4 dBZ within 30 min after $\tau = 75$ min) and they are located in the valley area. The horizontal wind speed achieves its peak value of 42.5 m/s for $\tau = 120$ min.

Reflectivity and flow patterns from Run A2 near the ground are plotted in Fig. 5a–f. Hereafter, the results are essentially different compared to Run

A1. So, the comparison of the echoes feature with/without orography indicates that the river valley is of the crucial importance for an individual Cb cloud development. For $\tau = 45$ min (Fig. 5a), more intense model cloud development compared to Run A1 (Fig. 3a) is observed. This is a consequence of the flat terrain that enables the free cloud lateral propagation. The peak

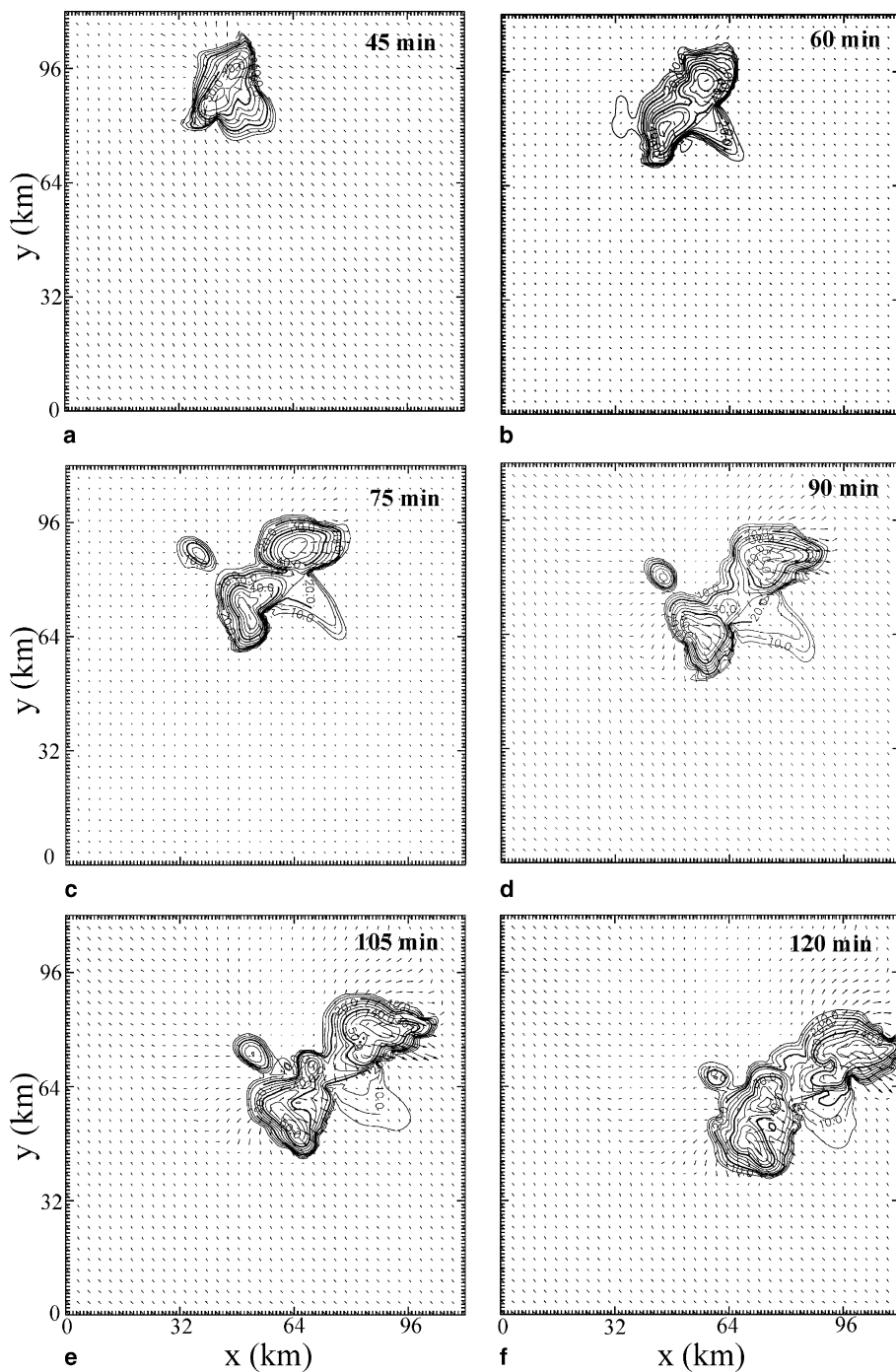


Fig. 5. As in Fig. 3, but for Run A2

reflectivity and the horizontal speed reach larger values (57.9 dBZ; 28.1 m/s) than for Run A1. Also, the maximum width of the radar echoe across to cloud motion is now for 15 km greater at $\tau=60$ min (Figs. 3b and 5b). Within next 15 min we can observe more than three times smaller reflectivity values at front part of the model cloud (Fig. 3c) than in Run A1 (Figs. 3c and 5c). This is due to the

absence of the front-side cell regeneration, and then smaller mother cloud propagation speed than for the valley case. New cells do not appear (Fig. 5c–f). Since the intense cloud growth starts earlier than in Run A1, the peak radar reflectivity of 59.3 dBZ is achieved for $\tau=60$ min. The peak horizontal wind speed is lower than in Run A1 (~ 35 m/s for $\tau=90$ min).

As follows from previous discussion, the river valley prevents warm and moist air transport from lateral direction. On the other side, it stimulates the mother cloud propagation along the valley axis. As a consequence, the cold nose layer is thicker along the storm propagation, which in turn, lead to the intense front-side cell

regeneration. For the flat terrain, the cold air diverges and the cold air nose is thinner. This can induce the absence of cell regeneration at the leading edge of the cold air outflow in contrast with prevailing theory (Browning, 1977; Lin et al, 1998). Initially the mother cloud propagates faster than in Run A1 due to smaller surface

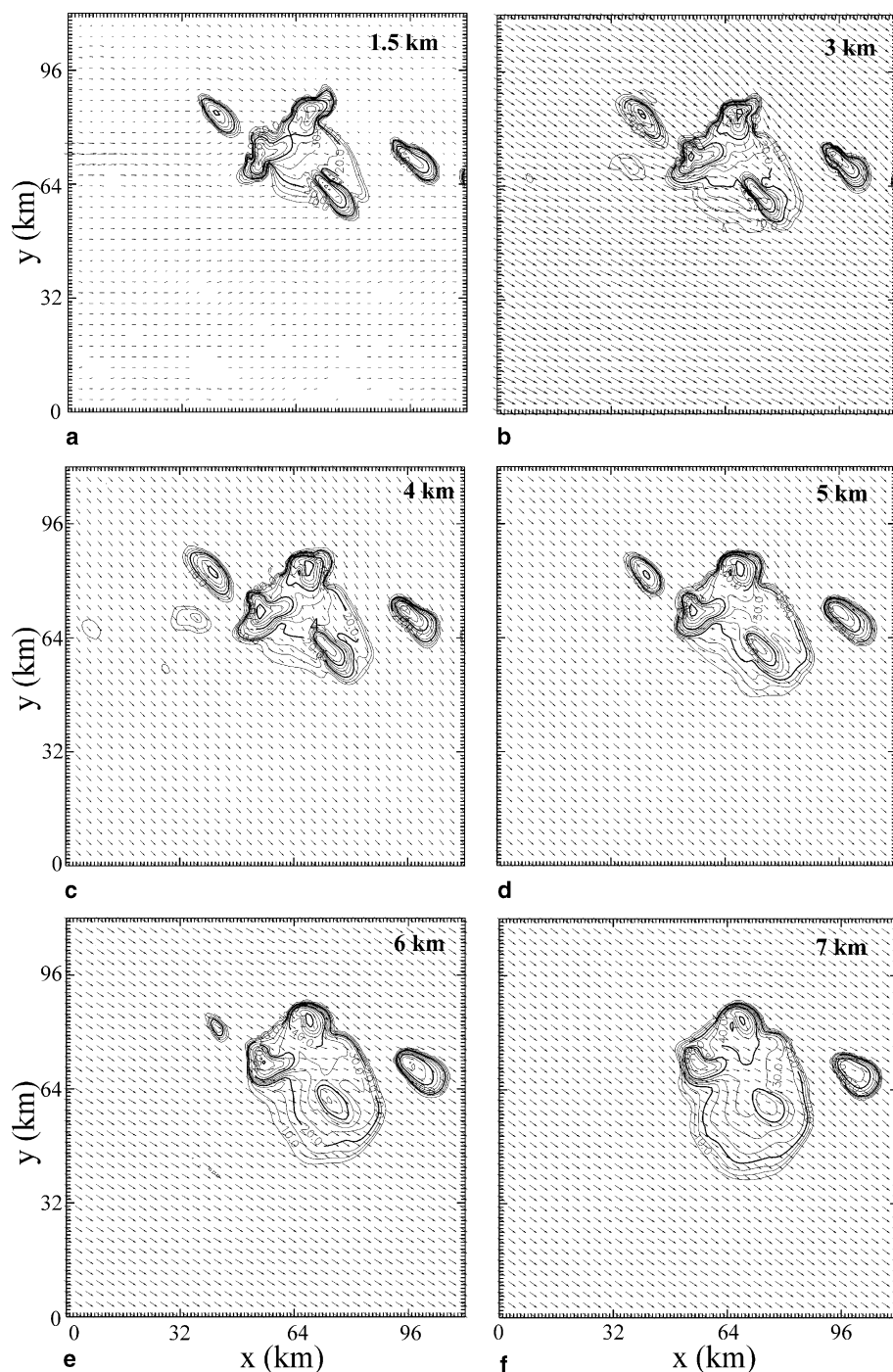


Fig. 6. Reflectivity and flow pattern depicted on selected horizontal planes at $\tau = 75$ min for Run A1. Figure 6a–f relates to levels of 1.5, and 3–7 km with a 1 km step, respectively. The axes x and y are in km

friction. Later, the absence of the cell regeneration lead to smaller cloud propagation speed compared to Run A1.

Our intention is also to point out the maximum differences of reflectivity patterns on horizontal plane and flow characteristics with altitude for runs A1 and A2. Therefore, we select horizontal planes of 1.5 km height and from 3–7 km with a

step of 1 km for $\tau = 75$ min (Figs. 6 and 7). Radar echoes area of the mother cloud enlarges within altitude from surface to 6 km and then decreases. There are three areas of increased reflectivity (Figs. 6 and 7) associated by cells “1”–“3”, whose intensity decreases above 4 km MSL (compare Fig. 6a–c and Fig. 6d–f). The cell behind the mother cloud does not propagate

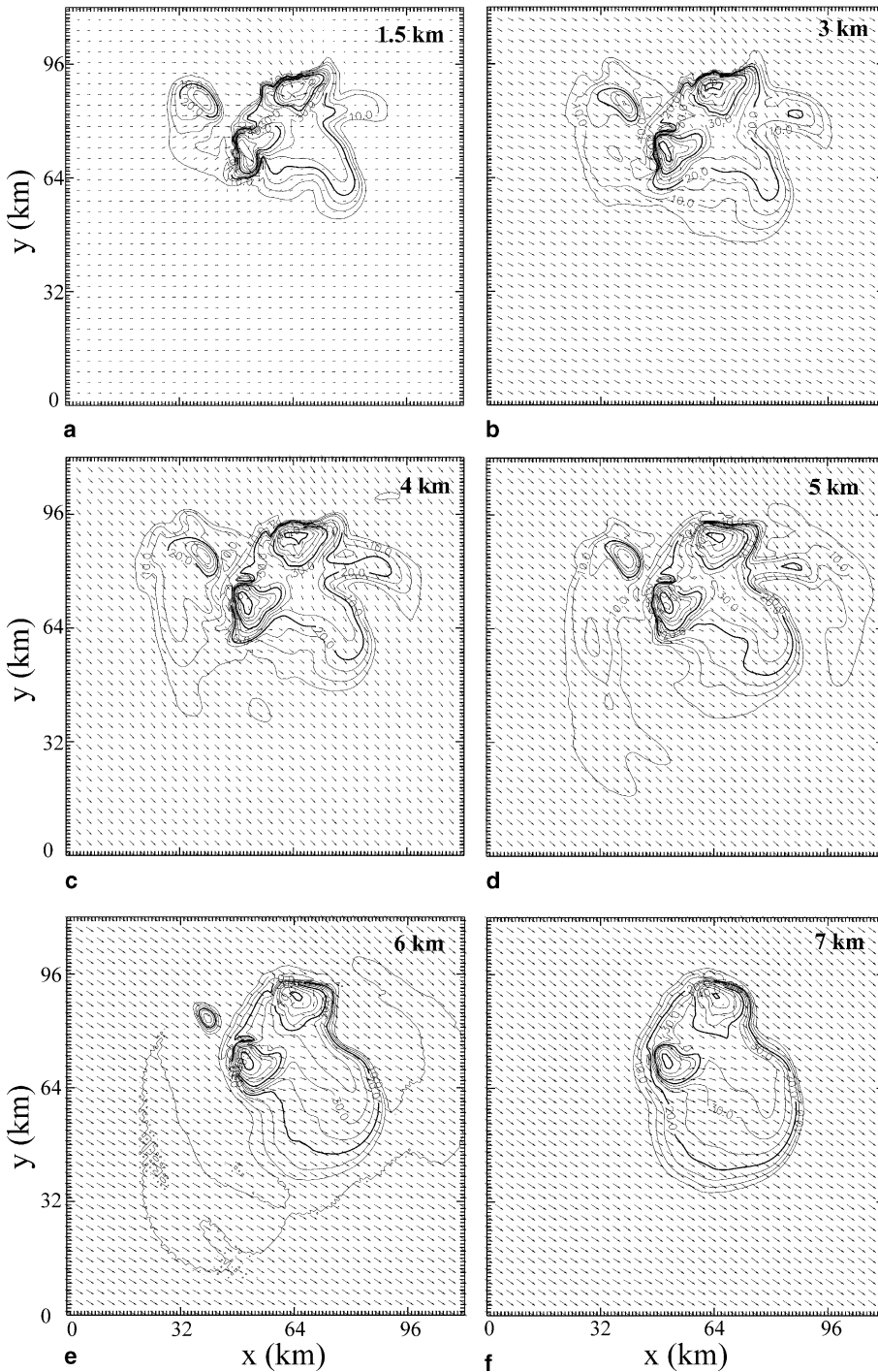


Fig. 7. As in Fig. 6, but for Run A2

above 6 km (Fig. 6e and f). Differences in reflectivity and flow patterns between runs A1 and A2 become more pronounced with altitude (Fig. 7). For Run A2 the radar echo area is larger than for Run A1 (Figs. 6a, b and 7a, b). Furthermore, for the flat terrain the cold air outflow beneath the mother cloud also spreads out in lateral direction. This induces the forced lifting of the warm moist air at the mother cloud flanks attaining

its condensation level at high levels. Therefore, the area with selected reflectivity has “bat like wings” for heights over 4 km (Fig. 7c–e). Such visual appearance are lost at 7 km (Fig. 7f).

Owing to the comparison of model and observed reflectivity structures of the Cb cloud, it is useful to show reflectivity and flow patterns in vertical cross-section through the storm (Fig. 8, Run A1). After $\tau = 45$ min (Fig. 8b–f) the peak

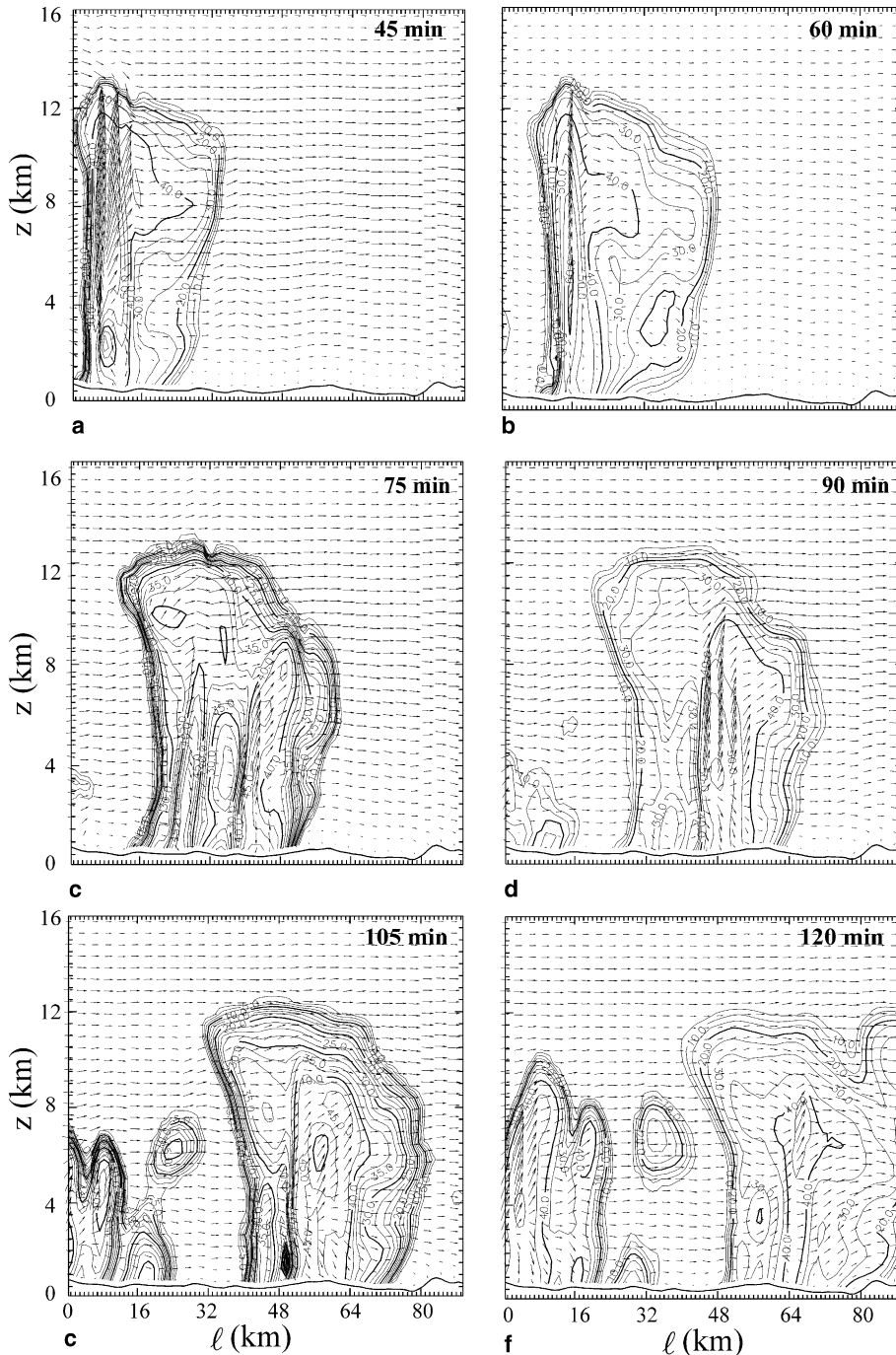


Fig. 8. Evolution of reflectivity (dBZ) and wind (m/s) in vertical cross-section through the storm for the same time intervals as in Fig. 3. The axes ℓ and z are in km

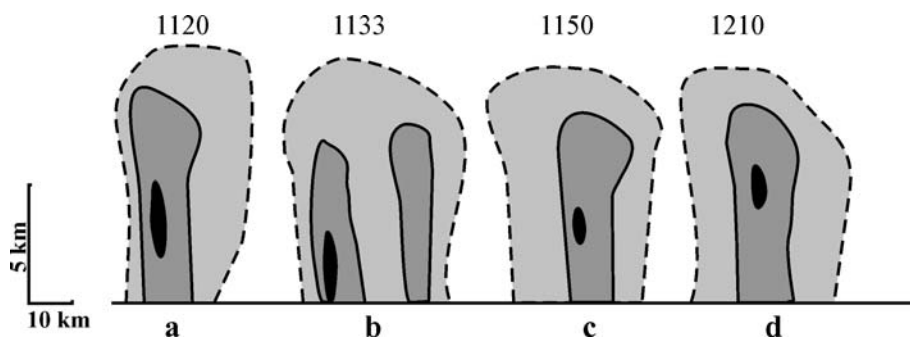


Fig. 9. Selected PPI scans for an individual Cb cloud observed in the Western Morava valley on 13th June, 1982. Shown PPI scans relate to direction along the valley axis for the next time intervals: **a** 1120; **b** 1133; **c** 1150, and **d** 1210 of local time. These time intervals correspond approximatively to those for model cloud after $\tau = 60$ min of simulated time. Radar echo isolines are 20 (dash line) and 40 dBZ (solid line). The black-coloured areas relate to radar reflectivity above: **a** 60 dBZ; **b** 45 dBZ; **c** 55 dBZ, and **d** 45 dBZ, respectively

values of reflectivity alternately decrease and increase in time (61.1, 49.7, 55.8, 47.4 and 51.1 dBZ). Such regular distribution of reflectivity is supported by observations. It can be explained by stronger and weaker forcing of the inflowing warm air through the mother cloud base (Ćurić, 1987). The flow pattern shows usual feature: the main updraft area is 10 km far from the front cloud boundary (Fig. 6a). At its back side there are downdrafts associated with the precipitation zone.

We now compare PPI scans of the air-mass Cb cloud observed on 13th of June 1982 in the Western Morava valley with corresponding reflectivity structure of the model cloud. All hail bearing clouds drifting over the Western Morava valley area are monitored by S band radar located near Užice (10 cm wave length radar). During the storm, the radar was operated rapidly, so that it was able to follow its evolution. Maximum values of radar reflectivity factors were reported each 3–5 min. For this purpose we select the PPI scans when the observed cloud attains more intense growth (Fig. 9). At 1120 of local time (corresponds to $\tau = 60$ min of simulated time) the Cb cloud already moves along the valley between Požega and Čačak (Fig. 9a). Afterwards, it propagates along the Western Morava valley. The last PPI scan (Fig. 9d) corresponds approximately to $\tau = 105$ min of simulated time. As can be seen, the model reproduces well some general characteristics of vertical reflectivity structure: radar top heights, location and values of reflectivity maxima.

Mountain influence on the areal characteristics of different types of convective precipitation is very important (Ćurić and Janc, 1992). We

therefore present model values of surface cumulative rain precipitation for Run A1 in Fig. 10. As noted, the area of cumulative rain precipitation has the wing-like form after $\tau = 60$ min of simulated time as a consequence of precipitation induced by the mountain sides. Since the storm develops and encircles larger area in horizontal with time, the enhancement of rain precipitation at the storm flanks can be observed (Fig. 10d–f). Two separate areas of precipitation with orientation along the valley axis occur at $\tau = 90$ min (Fig. 10d). They are denoted by A and B. The averaged mutual distance between area centers is about 30 km and it remains nearly unchanged with time (Fig. 10e–f). On the other side, the A and B areas continue to spread along the valley axes. It is evident that the B area is associated with the front-cell regeneration over cold air nose.

Such model areal characteristics of rain precipitation are supported by observations (Ćurić and Janc, 1982; 1992). Precipitation data are collected at the dense network of 235 rocket firing stations (mean distance between sites is 5 km) installed for hail suppression project. The observers report only a day when hail and other precipitation (ranged in nine classes) occur from Cb clouds at their stations. They do not measure rainfall amounts at each firing station because the hail suppression project is not designed for studies of detailed rainfall pattern. The analysis of Ćurić and Janc (1992) shows the existence of two separate areas with maximum of point frequencies for rain showers along the Western Morava valley. Their locations correlate well with the areas A and B simulated by the model.

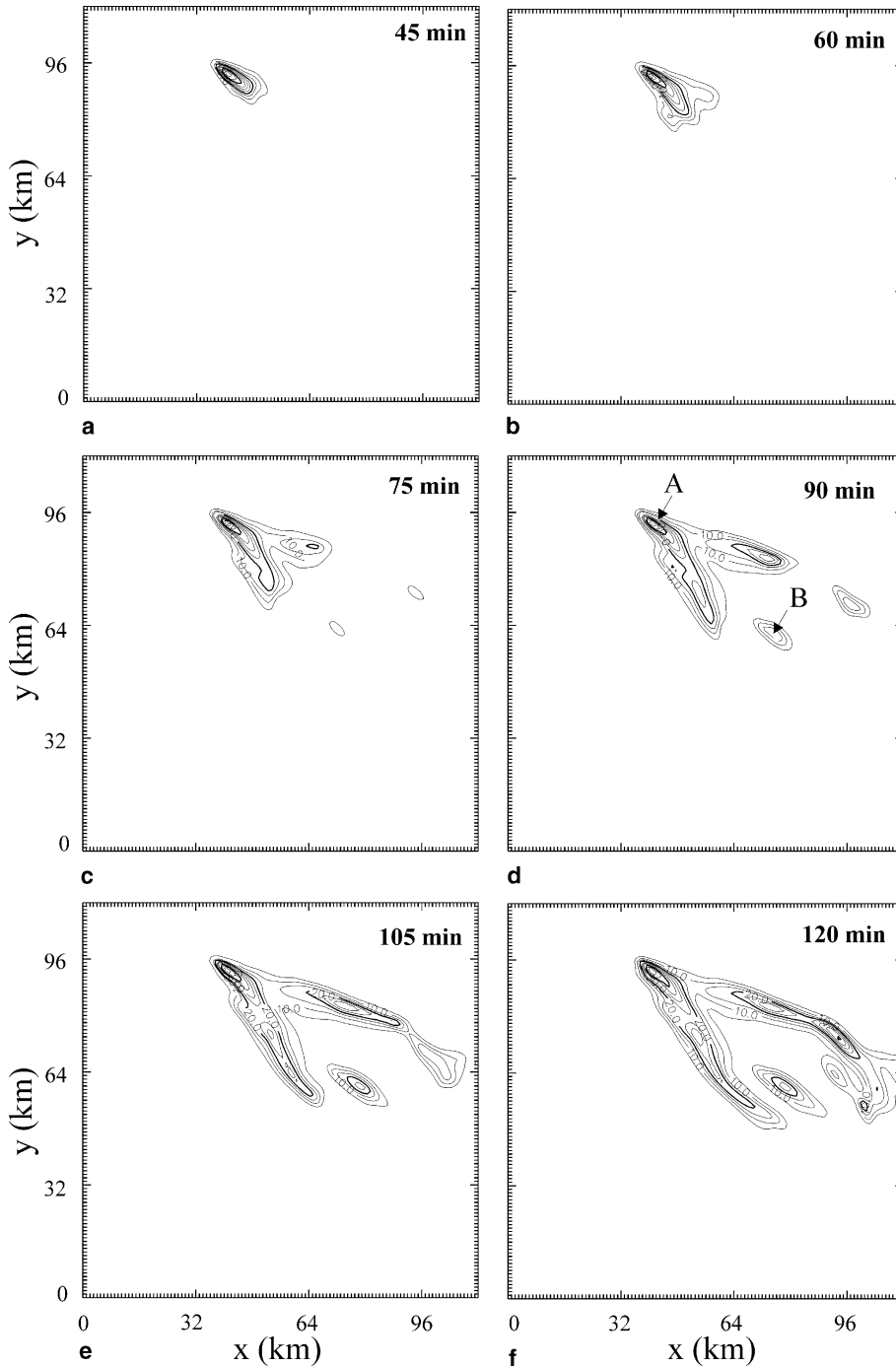


Fig. 10. Model values of surface cumulative rain precipitation (in mm) for Run A1 at time intervals as in Fig. 3. The areas denoted by A and B in Fig. 10d are discussed in the text

3.2 Case B

The model cloud is initialized after $\tau = 15$ min (graphics are not shown) for deep shear layer. It is intensified to 61 dBZ reflectivity after $\tau = 105$ min, while the peak values of updraft and downdraft speeds (29 and -7.2 m/s, respectively) are achieved for $\tau = 75$ min. Downdrafts are mainly located at the back part of the cloud. The cold air nose are formed at $\tau = 45$ min.

Now, the radar echoes encircle larger area than in case A. Low-level wind direction is backed by 180° with respect to the mean environmental wind. The intense storm development is influenced by deep layer of the opposite wind at low-levels, which in turn, prevents the cloud propagation towards the valley despite mid-tropospheric wind from NW-direction (Browning, 1977).

Table 1. The model values of some cloud parameters for experiments A1, A2, B and C

Cloud parameters	Experiments			
	A1	A2	B	C
Maximum reflectivity at horizontal plane near ground (dBZ)	57.4	59.0	61.0	52.9
Maximum reflectivity at vertical cross-section along ℓ -axis (dBZ)	61.1	63.3	65.2	52.4
Maximum updraft speed over cold air nose along ℓ -axis (m s^{-1})	15.0	29.0	27.7	/
Maximum updraft speed in vertical cross-section along ℓ -axis (m s^{-1})	27.6	29.0	29.0	10.2
Maximum positive helicity ($\text{m}^2 \text{s}^{-2}$)	551	553	338	91
Maximum negative helicity ($\text{m}^2 \text{s}^{-2}$)	303	460	351	170
Cloud base height (km)	1.5	1.0	2.0	2.0
Cloud top height (km)	13.5	13.5	12.5	11.5
Maximum cloud ice mixing ratio (g kg^{-1})	2.2	2.4	3.0	0.5
Maximum rainwater mixing ratio (g kg^{-1})	3.5	8.7	6.1	3.2

3.3 Case C

Case C is simulated under weak shear and the northwestern wind. According to Browning (1977), such hodograph is associated with short-lived storms, whose propagation essentially depends on mean environmental wind. Consequently, the model cloud becomes less intense and it moves somewhat further to the south compared to cases A and B. The storm intensity depends on initial perturbation. Peak reflectivity and updraft speed respective values of 52.9 dBZ and 10.2 m/s are achieved at $\tau = 30$ min. Storm decays within next 60 min.

Finally, we summarize some results of the experiments in Table 1. As noted, the helicity takes large values for A and B cases, in contrast with C one. Cloud top heights are the highest for A1 and A2 model runs. The maximum updraft over cloud air nose is greater in Run A2 compared to Run A1. This value relates to the stage of cloud life before the front-cell regeneration becomes expressed. Generally speaking, the strong wind shear is crucial factor for the cloud intensity as Table 1 clearly shows.

4. Conclusions

The model characteristics of an individual Cb cloud moving along a valley give more information of such a cloud and the orographic impact on its life cycle. The main results following the comparison of two model runs (A1 and A2) are as follows:

- (i) Real orography lead to the fast mother cloud propagation and well pronounced cell

regeneration at the leading edge of the cold air outflow. The river valley stimulates the cloud propagation along its axis, while it prevents that the cloud propagates freely in lateral direction. Inside the mother cloud, three cells are formed: one associated with forced updraft near leading edge of the cold air nose and two with the opposite sign of vorticity at flank storm sides. Their intensity decrease above 4 km height.

- (ii) Flat terrain generates quite different model cloud features. The mother cloud propagation speed is generally lower than for the real orography due to the weak expressed front-side regeneration. The cloud has more intense lateral development caused by free warm moist air transport as well as the cold air outflow propagation in lateral direction. The horizontal radar echoe area with the characteristic “bat-like” wings is much larger with altitude than in the valley case.
- (iii) The model cloud is sensitive to the change of shear at low-level. For deep shear layer, the simulated cloud is more intense than for shallow one. It cannot move far from the initiation place because the low-level wind from SE-direction prevents its motion towards the valley. The cloud simulated under weak shear condition does not move along the valley axis and it decays quickly.
- (iv) Model reflectivity structure agree well with its observed behavior. Areal characteristics of the rain precipitation induced by the real orography simulated by the model also correlate well with those observed.

References

- Browning KA (1977) The structure and mechanisms of hailstorms. Hail: A review of hail science and hail suppression. Meteor Monogr 38, Amer Met Soc, pp 1–43
- Ćurić M (1980) Dynamics of a cold air outflow from the base of the thunderstorm. A simple model. J Rech Atmos 14: 493–498
- Ćurić M (1982) The development of the cumulonimbus clouds which moves along a valley. In: Cloud dynamics (Agee EM, Asai T, eds.). Dordrecht: Reidel, pp 259–272
- Ćurić M (1987) Internal radar characteristics of Cb population in mountain region. Proc. XIIIth Inter. Conf. Carpathian Meteorology, September 14–19, 1987, Busteni-Romania, pp 133–140
- Ćurić M, Janc D (1992) Mountain influence on the areal characteristics of types of convective precipitation. Theor Appl Climatol 45: 71–76
- Ćurić M, Janc D (1996) Sensitivity of modeled hail accretion rates on the lower boundary of the hail spectrum. Meteorol Z, NF 5: 51–59
- Ćurić M, Janc D (1997) On the sensitivity of hail accretion rates in numerical modeling. Tellus 49A: 100–107
- Ćurić M, Janc D, Vučković V (1999) Verification of the improved predictive capability of a 1-D forced time-dependent cloud model with truncated hail spectrum. Meteorol Z, NF 8: 143–154
- Davies-Jones RP (1982) Tornado dynamics. Thunderstorm Morph Dyn 2: 297–361
- Droegemeier KK, Lazarus SM (1993) The influence of helicity on numerically simulate convective storms. Mon Wea Rev 121: 2005–2029
- Droegemeier KK, Xue M, Johnson K, O’Keefe M, Sawdey A, Sabot G, Wholey S, Mills K, Lin N-T (1995) Weather prediction: A scalable storm-scale model. In: High performance computing (Sabot GW, ed.), Addison Wesley, pp 45–92
- Fovell RG, Tan P-H (1996) Why multicell storms oscillate. Preprints 18th Conf. Severe Local Storms, San Francisco, CA, Amer Met Soc, pp 186–189
- Johnson KW, Bauer J, Riccardi GA, Droegemeier KK, Xue M (1994) Distributed processing of a regional prediction model. Mon Wea Rev 122: 2558–2572
- Lin Y-L, Deal RL, Kulie MS (1998) Mechanisms of cell regeneration, development and propagation within a two-dimensional multicell storm. J Atmos Sci 55: 1867–1886
- Lin Y-L, Joyce LE (2001) A further study of mechanisms of cell regeneration, development and propagation within a two-dimensional multicell storm. J Atmos Sci 58: 2957–2988
- Toutenhoofd V, Klemp JB (1983) An isolated cumulonimbus observed in northeastern Colorado: Comparison of field observations with results of a three-dimensional simulation. Mon Wea Rev 111: 468–478
- Xue M, Droegemeier KK, Wong W (2000) The Advanced Regional Prediction System (ARPS) – A multi-scale nonhydrostatic atmospheric simulation and prediction model. Part I: Model dynamics and verification. Meteorol Atmos Phys 75: 161–193
- Xue M et al (2001) The Advanced Regional Prediction System (ARPS) – A multi-scale nonhydrostatic atmospheric simulation and prediction model. Part II: Model physics and applications. Meteorol Atmos Phys 76: 143–165

Authors’ address: Mladjen Ćurić, Dejan Janc, Dragana Vujović and Vladan Vučković, Department of Meteorology, University of Belgrade, Serbia (E-mail: curic@ff.bg.ac.yu)